



Adaptive parallel reflex- and decoupled CPG-based control for complex bipedal locomotion



Chaicharn Akkawutvanich^a, Frederik Ibsgaard Knudsen^b, Anders Falk Riis^b, Jørgen Christian Larsen^{a,b}, Poramate Manoonpong^{a,b,*}

^a Bio-Inspired Robotics & Neural Engineering Laboratory, Information Science and Technology, Vidyasirimedhi Institute of Science and Technology, Rayong, Thailand

^b Embodied AI and Neurorobotics Laboratory, SDU Biorobotics, The Mærsk Mc-Kinney Møller Institute, University of Southern Denmark, Odense, Denmark

ARTICLE INFO

Article history:

Received 5 March 2020

Received in revised form 10 September 2020

Accepted 27 September 2020

Available online 30 September 2020

Keywords:

Bipedal walking robots

Central pattern generator

Adaptive online learning

Asymmetric gait

ABSTRACT

The achievement of adaptive, stable, and robust locomotion and dealing with asymmetrical conditions for bipedal robots remain a challenging problem. To address the problem, this paper introduces adaptive parallel reflex- and decoupled central pattern generator (CPG)-based control for a planar bipedal robot. The control has modular structure consisting of two parallel modules that work together. Firstly, as the main controller, the reflex-based control module inspired by an agonist–antagonist model, utilizes proprioceptive sensory feedback to adaptively generate various stable gaits. In parallel, as an auxiliary controller, the decoupled CPG-based control units individually governing the robot legs have the ability to learn the generated gaits in an online manner. Using the proposed framework, our study shows that this real-time control approach contributes to stable gait generation with robustness toward sensory feedback malfunction and adaptability to deal with environmental and morphological changes. Herein this study, we demonstrate the planar bipedal robot control functionality on a variable speed treadmill, dealing with asymmetric conditions such as weight imbalance and asymmetric elastic resistance in the legs. However, the approach does not require robot kinematic and dynamic models as well as an environmental model and is therefore flexible. As such, it can be used as a basis for controlling other bipedal locomotion systems, like lower-limb exoskeletons.

© 2020 Elsevier B.V. All rights reserved.

1. Introduction

Bipedal robot locomotion has been a subject of ongoing robotic research for over decades. Achieving adaptive, energy-efficient, and robust locomotion and dealing with asymmetrical conditions for bipedal robots are a challenging problem and have not been fully addressed. Many control techniques have been developed to govern bipedal robots either with the whole body (torso with upper and lower limbs) or the partial parts as lower limbs [1–4]. The techniques can be classified into two main approaches: (i) the engineering-based control approach, and (ii) the bio-inspired control approach. Our work focuses on the lower limb locomotion in the sagittal plane of the testing robot where the concept can be extended further to advance application such as an exoskeleton.

In the former approach, the kinematics/dynamics of the robot system needs to be precisely modeled to interact with the surrounding environment. A low-dimensional model such as the linear inverted pendulum was presented in Kajita et al. [5], Hong and Kim [6] and a high-dimensional model in Kuindersma et al. [7]. Apart from the kinematic model-based method for trajectory tracking used in the aforementioned models to form a stable walking pattern, Braun et al. [8] deployed the kinematic model-based method for state-dependent torque control. However, the complicated and time-consuming model optimization of the method makes it difficult for real-time implementation and online optimization or adaptation. With the machine learning technique, Tutsoy [9] developed reinforcement learning (RL) using a complete symbolic inverse kinematic solution to balance the lower body of a robot in the simulation. Their work showed promising results in learning to stabilize the upright position within ten seconds. However, real implementation is still a concern. Generally, the engineering-based (or model-based) control approach faces three main challenges when applying it to complex nonlinear dynamical systems, like bipedal robots. The

* Corresponding author at: Bio-Inspired Robotics & Neural Engineering Laboratory, Information Science and Technology, Vidyasirimedhi Institute of Science and Technology, Rayong, Thailand.

E-mail addresses: chaicharn.a_s17@vistec.ac.th (C. Akkawutvanich), poramate.m@vistec.ac.th (P. Manoonpong).

challenges include (i) maintaining an accurate model of uncertainty, (ii) reducing complexity to enhance computational efficiency, and (iii) increasing the control flexibility and adaptability to handle unpredictable and abrupt environmental changes. From this point of view, the bio-inspired control approach (such as the reflex model [10,11], central pattern generator (CPG) [12,13], or a combination of the two [14,15]) have received greater attention. This is because it does not require a precise robot dynamic and/or kinematic model or at all. It can be adaptive to deal with changing environmental conditions and robust against disturbances from the environment [16].

Regarding a reflex model, Geng et al. [10] developed the reflex-based neuronal network control of a bipedal robot. The control utilizes phasic feedback to successfully generate a dynamically stable biped walking gait. This reflex-based framework also contains modular features for interaction with other modules. The peripheral sensing modules could communicate with the core module through a synaptic plasticity mechanism for walking up a slope as demonstrated in Manoonpong et al. [17]. Another work by Geyer and Herr [11] demonstrates the influence of legged mechanics by encoding it into autonomous muscle reflexes. Their neuromuscular model resembles human locomotion with compliant leg behavior.

The implementation of CPG to achieve bipedal locomotion, the idea can be traced back to the work of Taga et al. [13]. A mathematical control model using a neural rhythm generator composed of several coupled neural oscillators (Matsuoka [18]) was proposed based on differential equations. It served as a signal generating center for a musculo-skeletal system based on Newton–Euler equations. Nonetheless, their model only showed a normal walking movement on a level floor in the simulation. Subsequently, Liu et al. [19] improved the model from Taga by introducing new coupling links between the knee and ankle oscillators. To obtain proper periodic patterns from the Matsuoka-based CPG network, one needs to search for proper control parameters or synaptic weights. This can be done by empirical exploration [20,21] and/or machine learning [22–26]. For example, Matsubara et al. [22] demonstrated a policy gradient method for reinforcement learning (RL) to tune appropriate sensory feedback to the CPG network. The method provided good performance in generating the locomotion of a planar 5-link biped robot. Subsequently, Tutsoy et al. [23] extended the method using a symbolic inverse kinematic model. Nakamura et al. [24] introduced a CPG-actor-critic RL method learning the CPG control parameters to generate locomotion in a simulated planar biped robot on different terrains. Yazdi and Haghhighat [25] proposed the Harmony Search (HS) algorithm to find the optimal synaptic weights of the CPG network to achieve fast bipedal walking of a simulated 3D NAO robot. Saputra et al. [26] employed a Genetic Algorithm (GA) to optimize the weights of the CPG network to acquire variant motion, including different walking directions for a 3D humanoid robot. Nonetheless, all the aforementioned employed machine learning frameworks are still restricted mainly to offline parameter tuning (i.e., learning through simulation before transfer to a real robot) and a number of trials. Therefore, it is impractical and sometimes impossible for the robot to deal with unexpected or unforeseen changes it has not learned before. Moreover, since the Matsuoka-based CPG network used is a reactive type, requiring constant feedback to maintain its entrained outputs for robust locomotion, missing feedback leads to unstable locomotion.

To achieve online parameter tuning of a CPG, Righetti et al. [27] introduced the Adaptive Frequency Oscillator (AFO) concept. It is an adaptive type framework consisting of an oscillator (or CPG) and an online dynamic Hebbian learning-based frequency adaptation mechanism. Santos et al. [28] applied the

AFOs to a simulated 2D bipedal model to achieve stable locomotion on changes among flat ground, climbing and descending surfaces. While the classical AFO framework shows online adaptation, it still requires a relatively long adaptation time. To obtain faster adaptation, Nachstedt et al. [29] proposed a novel online frequency adaption mechanism, called Adaptation through Fast Dynamical Coupling (AFDC). It is based on dynamically adapting the coupling strength of sensory feedback that modulates the frequency of a neural oscillator-based CPG.

The combination of a reflex-based network and CPG network is presented in many works. Dzeladini et al. [14] extended the neuromuscular model proposed by Geyer and Herr [11] with a model called feedforward and feedback based locomotion (3FBL), providing feedback predictors using morphed oscillators (CPGs) to modulate gait speed. In other words, they use the CPG-based control to modify the reflex-based control. In contrast, Canio et al. [15] also combine the two concepts, but exploit the reflex-based module to modify the CPG-based module via the AFDC mechanism, whereby the original signal is memorized. During the normal state, the two modules work in parallel, so when the reflex-based module fails, the CPG-based module dominates. Their design had benefit in terms of system stability and demonstrated adaptation property. It exploited the important of the combined feedforward CPG with sensory feedback to deal with unexpected disturbances and imperfect sensors [30]. Nevertheless, it was still limited to one CPG for controlling two legs. Thus, it cannot deal with asymmetric conditions (such as unbalanced-weighted and asymmetrical elastic-resistant legs) where each leg should adapt itself independently. From this point of view, we propose here a novel adaptive parallel reflex- and decoupled CPG-based control framework that fulfills this deficiency since at least two CPGs are required for both legs, where each of which controls each leg. The proposed control framework has a modular structure. It uses the reflex-based control module, inspired by an agonist–antagonist model with proprioceptive feedback, to adaptively generate various stable gaits. This control module acts as a default locomotion generator. In parallel, the decoupled CPG-based control module, consisting of two independent CPG units, can quickly learn the generated gaits in an online manner. It acts as an assistive controller to achieve robust locomotion to deal with sensor malfunction and the aforementioned asymmetric conditions.

By employing the proposed control, we can address here adaptive, stable, and robust locomotion generation without (i) robot kinematic and dynamic models as well as an environmental model, and (ii) offline CPG control parameter tuning. In principle, the control approach has the following advantages:

- It can act as real-time control and be practically implemented on a real bipedal robot system.
- It can generate stable locomotion, demonstrating robustness against sensory malfunction.
- It can perform online adaptation for an external perturbation such as speed variation on a treadmill (i.e., environmental change).
- It can handle an imbalance in physical conditions (weight, elasticity), causing an asymmetrical leg situation (i.e., morphological change).
- It is flexible due to modularity; i.e., one can use the control framework as a basis for controlling other bipedal locomotion systems, like lower-limb exoskeletons, for rehabilitation. Controlling the exoskeleton, the reflex-based control, which generates robot locomotion, can be replaced by human locomotion and the decoupled CPG-based control can learn the human locomotion to later assist the locomotion.

2. Materials and methods

2.1. Bipedal robot

Based on the previous work of Canio et al. [15], we have modified and improved a planar bipedal robot¹ using the conceptual structure of a human lower limb (Fig. 1). It is used here as an experimental platform. The robot structure is 0.27 m tall and consists of hips, upper legs, knees, lower legs, and feet (Fig. 1(a)). The legs are made from aluminum, a rigid and lightweight material. Each leg is separated into upper (11 cm in length) and lower (10 cm in length). The body dimensions are 10 × 7 × 6 cm (W × D × H). Four servo motors are used to drive the hip and knee joints (Fig. 1(b)). One leg weights approximately 26 g and the total body weight including motors is 520 g. Each of the hip motors can swing an upper leg forward and backward between around 120 and 60°. The knee motors with the lower legs in a straight position are marked as 180° and can rotate the lower legs backward up to 90°. There are sensors to measure those angles, namely the left/right hip joint angle sensor (θ_{LH}, θ_{RH}) and left/right knee joint angle sensor (θ_{LK}, θ_{RK}). The ankles are built with springs which can tolerate the walking impact. The feet are linked to foot contact sensors (LF, RF) which act as switches. When the feet are pressed, the status of the contact switch turns from off to on. We use a standard computer for control implementation with an update frequency of 20 Hz. The bipedal robot walks on a treadmill with a new aluminum support structure. The support structure consists of two triangular shapes fixed onto the treadmill. Two machine ring-like parts are attached to each side of the shapes and these are used to hold the shaft through rubber dampers in order to suspend the whole bipedal robot. The rubber allows the robot to move on a treadmill with less constraint, fixing the hips and the whole body to move in any direction.

2.2. Adaptive parallel reflex- and decoupled CPG-based controller

The controller for complex bipedal locomotion is based on the adaptive parallel neural control shown by the block diagram in Fig. 2. The controller is composed mainly of four main modules: (i) a sensory signal processing module; (ii) a reflex-based control module; (iii) a decoupled CPG-based control module; and (iv) a control selection module. The reflex-based part is the main controller using a neural network with feedback from all joint angle sensors ($\theta_{LH}, \theta_{RH}, \theta_{LK}, \theta_{RK}$) and foot contact sensors (LF, RF) to generate a walking gait. In contrast to previous work [15], a new flexible structure is introduced here, namely the decoupled CPG-based part. It acts as an auxiliary controller and is composed of two separated CPG units which individually receive angle information from the hip joint angle sensors (θ_{LH}, θ_{RH}) to control each left and right leg. This auxiliary part performs the online learning of the walking gait pattern from the main part, enabling the robot to use its signals to drive the system when needed, such as in the case of foot contact sensor failure, causing the main part to malfunction. Regarding the module inputs, the robot itself will generate feedback signals, which in this case are left/right hip joint angle (θ_{LH}, θ_{RH}), left/right knee joint angle (θ_{LK}, θ_{RK}), and left/right foot contact (LF, RF). The signals are then preprocessed through the sensory signal processing module such that they are suitable as inputs to each control module. Finally, the reflex-based and decoupled CPG-based control modules produce $Motor_{Reflex}$ and $Motor_{CPG}$ which are the driving motor signals, respectively. Subsequently, a control selection module makes a decision on which motor signal will be used to control the movement of the robot. In the following, we describe the four main modules:

¹ The robot design is based on the concept of the planar dynamic biped walking robot RunBot [17] with compliant ankles and flat feet [31].

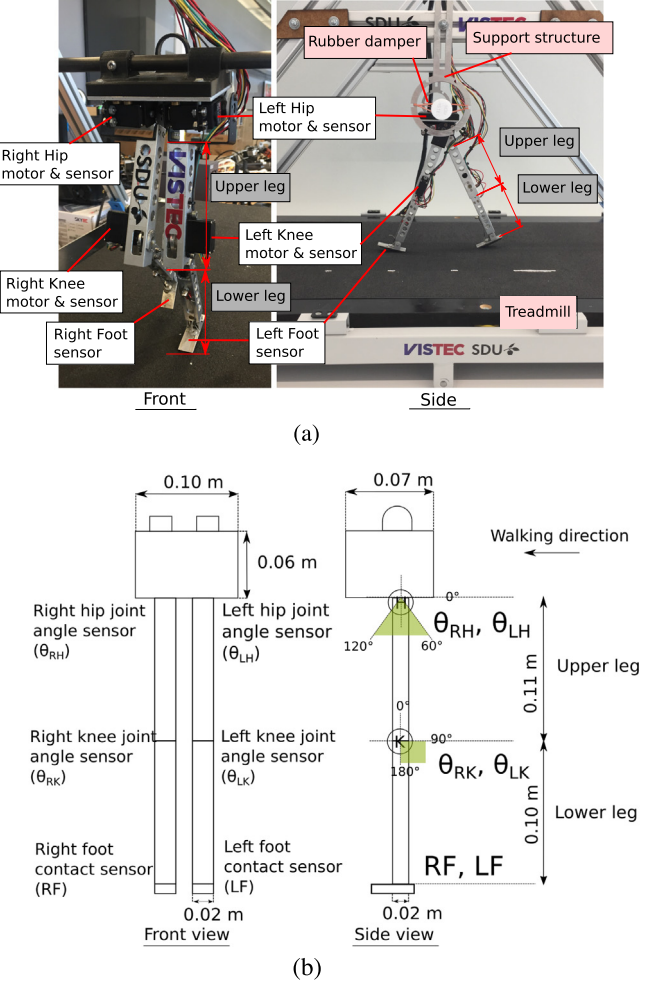


Fig. 1. The structure of the bipedal robot called “DACBOT”: (a) DACBOT with the support structure and rubber damper on a treadmill; (b) DACBOT’s sensors, namely left/right joint angle hip sensors (θ_{LH}, θ_{RH}), left/right joint angle knee sensors (θ_{LK}, θ_{RK}), and left/right foot contact sensors (LF, RF). The angle operation range of each hip motor is around 30° in both forward and backward directions, and each knee motor is only 90° in the backward direction.

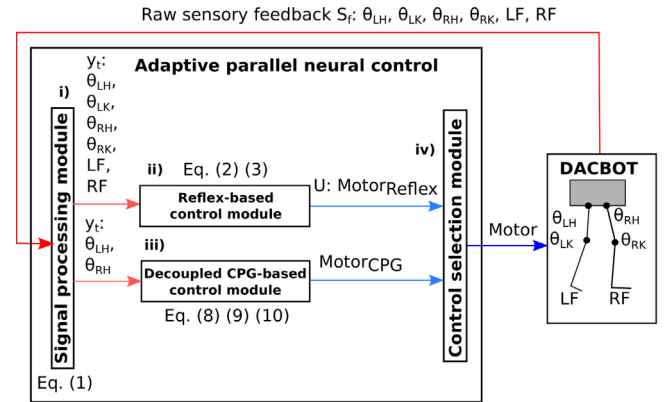


Fig. 2. Flow of information between the robot and control module. The sensors (Red lines) used to measure feedback signals from the “DACBOT” bipedal robot consist of: the left/right hip joint angle sensor (θ_{LH}, θ_{RH}), the left/right knee joint angle sensor (θ_{LK}, θ_{RK}), and the left/right foot contact sensor (LF, RF). The driving motor signals (Blue lines) for hips and knees ($Motor_{LH}, Motor_{LK}, Motor_{RH}, Motor_{RK}$) come from our adaptive parallel reflex- and decoupled CPG-based control module. Signals are selected from either the reflex-based ($Motor_{Reflex}$) or decoupled CPG-based ($Motor_{CPG}$) module. (For interpretation of the references to color in this figure legend, the reader is referred to the web version of this article.)

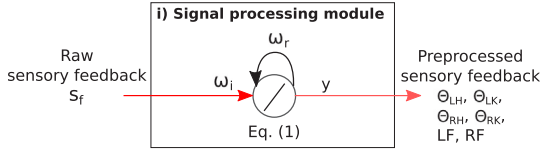


Fig. 3. Signal processing. The recurrent neural structure is used to filter noise from the raw sensory feedback.

2.2.1. Sensory signal processing module

To achieve a closed-loop control, signals from the joint angle and foot contact sensors are retrieved as sensory feedback. The joint angle signals are used as a reference pattern for the CPG-based units, whereas the foot contact signals initiate the reflex-based unit to generate a proper rhythmic gait. These raw signals are then preprocessed to reduce the noise emanating from hardware imperfection by using low pass filter neurons as shown in Fig. 3. These can be defined as follows: (1). ω_i represents the weight of input connection, ω_r represents the weight of recurrent connection from the previous output to current input, s_f represents the raw sensory feedback, and y represents the output after filtering ($\theta_{LH}, \theta_{LK}, \theta_{RH}, \theta_{RK}, LF, RF$).

$$y_t = y_{t-1}\omega_r + s_f\omega_i \quad (1)$$

where $\omega_i = 0.2$ and $\omega_r = 0.8$. This preprocessed sensory feedback is subsequently transmitted to the reflex-based control module and the decoupled CPG-based control module.

2.2.2. Reflex-based control module

The neural structure is designed to mimic the reflex mechanism in human-like walking, receiving a sensory signal to actuate movement. This structure becomes our main reflex-based control module, implemented earlier in our previous work [17]. The diagram in Fig. 4 shows this module with its real-time signals in Fig. 5(a) and its matched sequential movement in Fig. 5(b). All preprocessed sensory feedback ($\theta_{LH}, \theta_{LK}, \theta_{RH}, \theta_{RK}, LF, RF$) is utilized as input into this reflex-based control module. The module has a hierarchical structure consisting of two levels: top and bottom. The top level is a distributed neural network comprising hip anterior extreme angle neurons, ground foot contact sensor neurons, and interneurons which additionally command the motor neurons. The bottom level has motor neurons which directly drive the motors and joint angle sensor neurons [17].

The walking pattern is triggered by reflex-like actions generated from the reflex-based control module. The left (right) ground foot contact sensor neuron GL (GR) receives signals from the left (right) foot contact sensor LF (RF) and initiates its own leg in the hip's flexor reflex interneuron (FI), further triggering the hip's flexor motor neuron (FM) and inhibiting the hip's extensor motor neuron (EM). Together with information from the hip's flexor sensor neuron (FS), the hip's FM blends the upper leg backward. Whereas, the extensor reflex interneuron (EI) and extensor sensor neuron (ES) of the knee inform its EM to push the lower leg forward. The result is the stance leg on the side where its foot makes contact with the ground; in this case the left side. On the other leg, the hip's EI will signal further to hip's FM hip inhibiting flexion activity and to hip's EM activating extension activity. This is to lift the upper leg from the ground, while the knee's FI and FS inform the knee's FM to bend the lower leg backward to guarantee that the foot is in the air (see Fig. 5).

To prepare the lower leg to properly touch the ground again through limiting backward bending, the stretch receptor is introduced to measure the AEA. When the hip's angle reaches the AEA, the anterior extreme angle neurons in each leg (AL/AR), in this case AR, will trigger and send an inhibition signal, so that the

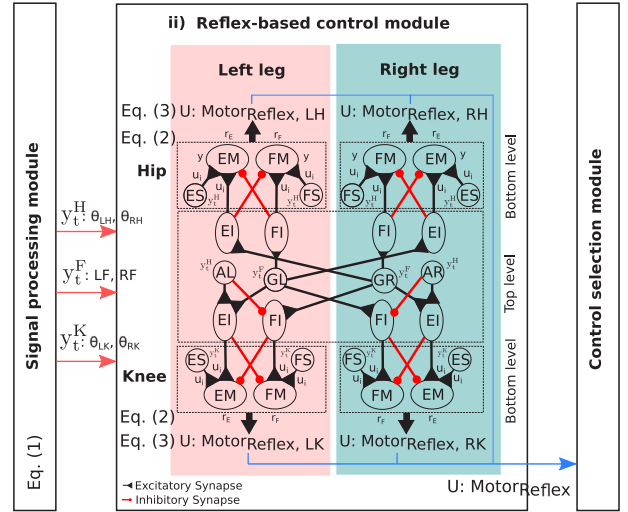


Fig. 4. The reflex-based control module. The block diagram shows the utilization of both joint angle and foot contact switch information. Each joint angle is measured by extensor/flexor sensor neurons (ES/FS) at the hip and knee, while the footstep is measured by the ground foot contact sensor neurons (GL/GR). The anterior extreme angle (AEA) is a hip angle measured by left and right (AL/AR) neurons. The main neurons for driving the motors are extensor/flexor motor neurons (EM/FM) in each hip and knee whereas extensor/flexor reflex interneurons (EI/FI) facilitate communication between the legs.

knee stops flexing and extends the lower leg forward again while it is still in the air. Subsequently, this swing leg makes contact with the ground and exchanges its role with the current stance leg. The same sequence starts again with the GL of the right leg as the initiator (see Fig. 5). The walking pattern generated by this method shows stability which is defined as the clear and repeatable stance-swing phase of each leg over a certain period of time. This can be seen from a gait diagram (Fig. 5(b)). This information can indicate walking without falling of the robot.

Each motor neuron has its own sensor neurons for measuring the joint angle in order to control it. The state and output of each motor neuron are governed by (2a) and (2b) [17]:

$$\tau \frac{dy}{dt} = -y + \sum \omega_i u_i, \quad (2a)$$

$$r = \frac{1}{1 + e^{-\alpha_N(y - \theta_N)}} \quad (2b)$$

where u_i represents the input into this motor neuron which comes from the output of the sensor neurons and interneurons, ω_i represents the connection strength of each input, τ is a time constant associated with the passive properties of the cell membrane (here it is set to 1), and y represents the mean membrane potential of the neuron. The (2b) is a sigmoid function where α_N is a positive constant (here it is set to 1), θ_N is a bias constant that controls the firing threshold (here it is set to 5), and r is output.

The voltage of the motor U is determined by:

$$U = G(\zeta_E r_E + \zeta_F r_F) \quad (3)$$

where U is the motor output in the voltage unit. G represents the converting gain (here it is set to 2.2). ζ_E and ζ_F are the signs for the motor voltage of the extensor and flexor, namely +1 or -1. r_E and r_F are motor neuron outputs. Further details of the equations can be seen in Manoonpong et al. [17].

2.2.3. Decoupled CPG-based control module

Apart from the reflex-based module where the system has to rely on the sensory signals to achieve the proper rhythmic pattern, the CPG-based concept is proposed here as an alternative

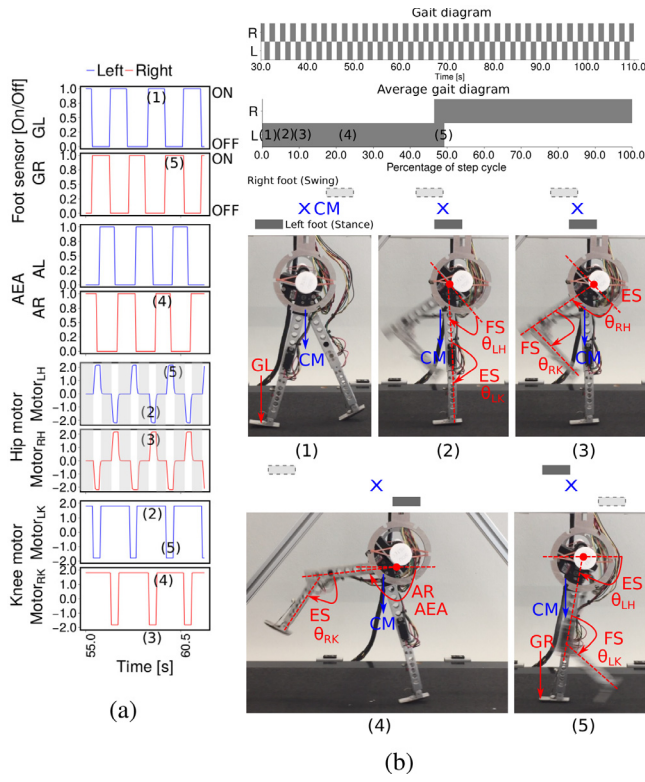


Fig. 5. (a) The real-time data of the reflex-based control module. The bipedal gait can be seen from the foot sensor signals of left leg (blue) and the right leg (red). Moreover, the driving motor signals generated by this reflex-based control module are also shown here as hip and knee motor signals. These driving signals show minimal energy consumption during periods of zero voltage (gray areas). (b) Snapshots of one stable walking step controlled by the reflex-based control module. The gait diagram shows a repeatable, steady-state pattern with variability (i.e., walking without falling) over a certain period of time (80 s). The average gait diagram clearly concludes the average walking pattern per cycle, indicating steady walking behavior, as evidenced by the clear stance-swing phase of each leg over a certain period of time. Firstly, in the time frame (1), the GL is activated, triggering the flexor of the hip joint and the extensor of the knee joint in this left leg (2). Later in the time frame (3), the right leg begins to swing, triggered by the extensor of the hip joint. Meanwhile its knee joint flexes to lift the whole leg over the floor. When the stretch receptor (AEA signal) of the swing leg is activated, its knee extensor moves the lower leg outward (4). Finally, in (5), the swing leg touches the ground, initiating the other stance leg with the same sequence. (For interpretation of the references to color in this figure legend, the reader is referred to the web version of this article.)

oscillating source. The CPG unit can memorize the reference signal emanating from the reflex-based module and continuously drives the system onward. When the robot walks in different conditions, the output signal of this CPG unit can automatically learn and adapt to this change. We propose here two uncorrelated CPG units to control each leg individually under the decoupled CPG-based control module of our developed system (see Fig. 6). It comprises two sets of oscillators and post-processing units. This concept, involving two independent control units handling each leg, is different from Canio et al. [15] where only one CPG receives the specific feedback from one leg in order to control both legs. The new design of two independent CPGs allows more flexibility in implementing the robot system where each of CPG obtains feedback from the corresponding leg. The module acquires only the preprocessed hip joint angle signals (θ_{LH} , θ_{RH}) as sensory feedback. They are then transformed into an appropriate scale as inputs ($F_{CPG, L}$, $F_{CPG, R}$) into the decoupled adaptive neural oscillators. Although decoupled during the learning process, the CPGs are implicitly coupled through mechanical coupling, leading to proper synchronization between two legs.

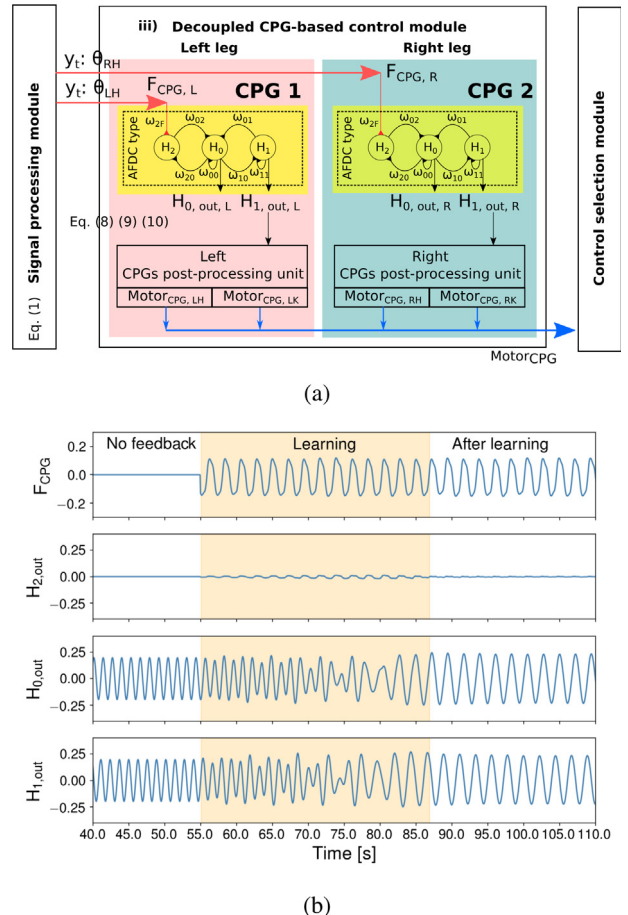


Fig. 6. The decoupled CPG-based control module. (a) Two independent AFDC-based CPG units (CPG 1 and CPG 2). Each receives only the left/right hip angle as input. The output signal $H_{1, out}$ is suitably postprocessed to generate the driving motor signal. (b) Example of the signals for one AFDC-based CPG unit. The output signals are produced from each neuron ($H_{2, out}$, $H_{0, out}$, $H_{1, out}$). When external input (F_{CPG}) occurs from sensory feedback, the internal neural frequency changes according to the input frequency (after the orange region).

Adaptation through Fast Dynamical Coupling (AFDC) works as our adaptive neural oscillators with synaptic plasticity. This neural mechanism shows faster adaptation compared to the Adaptive Frequency Oscillator (AFO) introduced by Righetti et al. [27].

The AFDC is derived from the SO(2) neural network [32] with an additional synaptic plasticity mechanism. The SO(2) structure has two neurons H_0 and H_1 with interconnections governed by ω_{01} and ω_{10} and self-connections ω_{00} and ω_{11} . The sensory feedback as an input (F_{CPG}) to the network via ω_{2F} to an extra synaptic neuron H_2 , attaching to the H_0 neuron via synaptic connections ω_{02} and ω_{20} . Conventionally, all connections are written with excitatory symbols and all weights can be either positive or negative. When the weight is positive, the excitatory connection occurs and when negative the inhibitory connection occurs. From the SO(2) neural network as part of the AFDC, we get activation equations at time t:

$$\begin{bmatrix} H_{0, act}(t+1) \\ H_{1, act}(t+1) \end{bmatrix} = \begin{bmatrix} \omega_{00}(t) & \omega_{01}(t) \\ \omega_{10}(t) & \omega_{11}(t) \end{bmatrix} \begin{bmatrix} H_{0, out}(t) \\ H_{1, out}(t) \end{bmatrix} + \begin{bmatrix} B_0(t) \\ B_1(t) \end{bmatrix}, \quad (4)$$

where $B_0(t)$ and $B_1(t)$ are biases. $H_{0, act}$ and $H_{1, act}$ represent the activity at each neuron. The outputs $H_{0, out}$ and $H_{1, out}$ are given by passing the activity through the hyperbolic tangent transfer

function:

$$\begin{bmatrix} H_0, \text{out}(t) \\ H_1, \text{out}(t) \end{bmatrix} = \begin{bmatrix} \tanh(H_0, \text{act}(t)) \\ \tanh(H_1, \text{act}(t)) \end{bmatrix}. \quad (5)$$

As proven previously in Pasemann et al. [32], this structure produces quasi-periodic output when the weights are according to

$$\begin{bmatrix} \omega_{00}(t) & \omega_{01}(t) \\ \omega_{10}(t) & \omega_{11}(t) \end{bmatrix} = \alpha \begin{bmatrix} \cos(\phi) & \sin(\phi) \\ -\sin(\phi) & \cos(\phi) \end{bmatrix} \quad (6)$$

with $-\pi < \phi < \pi$, $\alpha > 1$. Parameter ϕ determines the oscillation frequency and it is usually fixed to one value meaning that all weights are fixed. The phase shift between two outputs is $\pi/2$ where H_1, out leads when $\phi > 0$. For $\alpha = 1 + \epsilon$, $\epsilon \ll 1$, both outputs are almost sine-shaped with a small amplitude.

In this study, initialized values in (4)–(6) are chosen so that the output signals (see Fig. 6(b)) are in the oscillation region (Neimark–Sacker bifurcation) according to the previous work [32]. The biases and outputs are set to $B_0 = 0$, $B_1 = 0$, $H_0, \text{out} = 0.2$, $H_1, \text{out} = 0.2$ in order to initiate oscillation. The selection of parameter $\alpha = 1.01$ helps to yield an almost proportional relationship between ϕ and the oscillation frequency f . In our case, the ϕ is set to an arbitrary value (e.g., $\phi = 0.08\pi$). With this value, the system has an initial frequency of 0.125 (periodic) cycles per iteration step, approximately equals to 0.7 Hz in the real world.

If the network is modified by linking the external input F_{CPG} via an additional neuron, then it becomes the AFDC.

The frequency adaptation relating to the external input is governed by the following equations. Firstly, F_{CPG} influences the synaptic neuron H_2 , producing output $H_{2, \text{out}}$ at time t as we can see in

$$H_{2, \text{act}}(t+1) = \omega_{20}(t)H_{0, \text{out}}(t) + \omega_{2F}(t)F_{\text{CPG}}(t) + B_2(t), \quad (7a)$$

$$H_{2, \text{out}}(t) = \tanh(H_{2, \text{act}}(t)), \quad (7b)$$

where B_2 is bias and set to 0, initialized values of $\omega_{20} = 0$ ($\omega_{20}(0)$ or $\omega_{20,0}$), $\omega_{2F} = 0.01$ ($\omega_{2F}(0)$ or $\omega_{2F,0}$), and $H_{2, \text{out}} = 0.2$. Summarized equations for all outputs of one AFDC are shown below:

$$\begin{bmatrix} H_0, \text{act}(t+1) \\ H_1, \text{act}(t+1) \\ H_2, \text{act}(t+1) \end{bmatrix} = \begin{bmatrix} \omega_{00}(t) & \omega_{01}(t) & 0 \\ \omega_{10}(t) & \omega_{11}(t) & 0 \\ \omega_{20}(t) & 0 & \omega_{2F}(t) \end{bmatrix} \times \begin{bmatrix} H_0, \text{out}(t) \\ H_1, \text{out}(t) \\ F_{\text{CPG}}(t) \end{bmatrix} + \begin{bmatrix} B_0(t) \\ B_1(t) \\ B_2(t) \end{bmatrix}, \quad (8a)$$

$$\begin{bmatrix} H_0, \text{out}(t) \\ H_1, \text{out}(t) \\ H_{2, \text{out}}(t) \end{bmatrix} = \begin{bmatrix} \tanh(H_0, \text{act}(t)) \\ \tanh(H_1, \text{act}(t)) \\ \tanh(H_{2, \text{act}}(t)) \end{bmatrix}. \quad (8b)$$

Secondly, the online frequency adaptation is achieved by changing ϕ . This accords with the Hebbian-type learning rule based on the correlation $H_{2, \text{out}}$ as in

$$\Delta\phi(t) = \mu\omega_{02}(t)H_{2, \text{out}}(t)\omega_{01}(t)H_{1, \text{out}}(t), \quad (9)$$

where μ is the learning rate. The weights of these additional synapses ω_{2F} , ω_{02} , and ω_{20} also learn to change, based on the same rule, as shown in the following equation:

$$\begin{bmatrix} \Delta\omega_{02}(t) \\ \Delta\omega_{20}(t) \\ \Delta\omega_{2F}(t) \end{bmatrix} = \begin{bmatrix} -H_{0, \text{out}}(t)H_{2, \text{out}}(t) & -(\omega_{02}(t) - \omega_{02,0}) \\ -H_{0, \text{out}}(t)H_{2, \text{out}}(t) & -(\omega_{20}(t) - \omega_{20,0}) \\ F_{\text{CPG}}(t)H_{2, \text{out}}(t) & -(\omega_{2F}(t) - \omega_{2F,0}) \end{bmatrix} \begin{bmatrix} A \\ B \end{bmatrix}, \quad (10)$$

where $\omega_{02,0}$ (or $\omega_{02}(0)$), $\omega_{20,0}$ (or $\omega_{20}(0)$), and $\omega_{2F,0}$ (or $\omega_{2F}(0)$) are predefined relaxation values. The parameters $A, B > 0$ quantify

Table 1

Table of the four movement stages of the upper and lower legs.

		Stage 1	Stage 2	Stage 3	Stage 4
Upper leg	Left hip	+	0	-	0
	Right hip	-	0	+	0
Lower leg	Left knee	-	+	+	+
	Right knee	+	+	-	+

+ = Extension, - = Flexion, 0 = No drive.

the strength of each term. Based on the previous study [29], choosing $\mu = 1.0$ in (9) and $A = 1.0$, $B = 0.01$, $\omega_{02,0} = 1.0$, $\omega_{20,0} = 0$, and $\omega_{2F,0} = 0.01$ in (10) yields a proper adaptation. This synaptic plasticity can be considered as a short-term adaptation. Their weights are temporarily changed. When the desired frequency is reached, the synaptic weights ω_{02} , ω_{20} , ω_{2F} are back to their initial values. At first, the input F_{CPG} and the output $H_{0, \text{out}}$ are different. In (7a), the input F_{CPG} dominates the output $H_{2, \text{out}}$, strengthening the synaptic weights ω_{2F} , ω_{20} and decaying ω_{02} . $H_{2, \text{out}}$ drives the change in frequency through (9). As soon as the frequency has adapted to the external frequency i.e., adaptive frequency adaptation,² output $H_{2, \text{out}}$ and $H_{0, \text{out}}$ are highly correlated. This makes ω_{02} at its lowest value and ω_{20} at its highest value. At this point, $H_{0, \text{out}}$ almost fully compensates for the external input in (7a), resulting in the disappearance of $H_{2, \text{out}}$, and as a consequence, all synaptic weights ω_{02} , ω_{20} , ω_{2F} decay back toward their relaxation/initial values ($\omega_{02,0} = 1.0$, $\omega_{20,0} = 0$, and $\omega_{2F,0} = 0.01$).

The output signals $H_{0, \text{out}}$ and $H_{1, \text{out}}$ are illustrated in Fig. 6(b) where $H_{1, \text{out}}$ leads $H_{0, \text{out}}$ by 90° . The input signal F_{CPG} at a certain frequency urges the synaptic input H_2 neuron to produce a small $H_{2, \text{out}}$ amplitude during the frequency transition period. The internal frequencies of output signals $H_{0, \text{out}}$ and $H_{1, \text{out}}$ then adapt to the input frequency after a few seconds. After the learning phase is completed, the $H_{2, \text{out}}$ signal disappears. For this type of oscillator, even though the input is not persistently present, the network has already recognized the frequency and can maintain its last adaptation. Due to its leading phase behavior in relation to the input F_{CPG} , this advance in control signal is beneficial in compensating for the delay from the input to the system response.

In order to generate motor control signals to match the four movement stages of the upper and lower legs (see Table 1), the sinusoid $H_{1, \text{out}}$ is selected and separated into four sections according to its first derivative. The driving motor signals are then generated.

2.2.4. Control selection module

As previously stated, the main reflex-based control module generates the Motor_{Reflex} to primarily drive the walking robot and the decoupled CPG-based control module generates the Motor_{CPG} as the auxiliary module to supply signals when the main module fails. In order to make the transition between these two signals, we make conditions such that when there are no foot contact signals (LF, RF), motors are driven by signals from the decoupled CPG-based control module. For a non-disruptive transition period, the coherence between Motor_{Reflex} and Motor_{CPG} signals is monitored through its phase before the switching occurs.

3. Experimental results

We performed experiments to verify several important points: (i) Our proposed adaptive neural control mechanism; a reflex-based parallel with decoupled CPG-based control, can generate

² The adaptation shows the ability to memorize the influence of an external frequency, even when it has been removed.

the proper gait for our robot in normal conditions such as when the robot moves with symmetrical legs and all sensory feedback signals are functional. (ii) We tested the robustness of our system when some sensory feedback signals malfunctioned. Our planar bipedal robot can walk on a sagittal plane and its walking stability will be observed in this direction, whereas other dimensions are restricted by the support structure and damper. (iii) Rapid and online adaptation to external perturbation is another key feature of our control module which will be verified through walking on different speeds of a treadmill. (iv) Naturally, humans can walk with different leg properties. Their legs can be dissimilar in weight or one leg can experience muscular atrophy, so that the elasticity in each leg is not equal. We simulate these imbalances and asymmetrical elastic resistance conditions with our robot and observe the adaptability of the control module. The results are shown in the following section.

3.1. Symmetric conditions

The symmetric-legged condition is one in which two legs are physically the same.

3.1.1. Gait generation

In order for the robot to walk, it is important that the motor driving signal forms an appropriate pattern. The reflex-based control module can satisfy this requirement by generating a suitable bipedal gait. The following experiment demonstrates the ability of the module. The robot was placed on a treadmill and the speed fixed to a certain constant value. The experiment began solely with the activation of the reflex-based control module; the results of which are shown in Fig. 7. During walking, the foot contact sensors (LF, RF) of the robot generated foot sensor signals (GL, GR), hip joint angle sensors generated hip sensor signals (θ_{LH} , θ_{RH}), and knee joint angle sensors generated knee sensor signals (θ_{LK} , θ_{RK}) as inputs to the module. The hip and knee motor signals ($Motor_{LH}$, $Motor_{RH}$, $Motor_{LK}$, $Motor_{RK}$) were generated by the module to drive the robot. These motor signals were created cycle per cycle continuously as long as the robot moved forward with its left and right leg swinging alternately and repetitively. From the experiment, it is obvious that the robot can walk steadily in the presence of the relative sensors, as evidenced by the pattern of the motor signals. Furthermore, this steady walking pattern can also be clearly seen from the gait diagram, indicating the time taken for each foot to touch the ground (i.e., clear swing and stance phases). The pitch speed of the inertial measurement unit (IMU) in the robot walking direction also shows the separation between steady and failed walking. Nevertheless, following sensor malfunction (i.e., with foot contact sensors turned off and hip and knee sensor signals set to certain values), this control module could not generate proper motor driving signals. Therefore, both robot legs were paralyzed and it was unable to walk.

To verify the robustness of our proposed adaptive parallel reflex- and decoupled CPG-based control module, the experiment was set up in such a way that the bipedal robot walked for 55 s (approximately 16 walking steps) with the reflex-based control mechanism and the decoupled CPG-based control subsequently learned the pattern and frequency from the feedback signals emanating from each left and right hip sensor (θ_{LH} , θ_{RH}). After 110 s, the signals from the decoupled CPG-based control mechanism were utilized, with all foot contact sensors (LF, RF) switched off and hip sensor signals (θ_{LH} , θ_{RH}) set to certain values. This result is shown in Fig. 8.

In principle, the decoupled CPG-based control module and the reflex-based control module are actually active, working as a backup system by being on standby and monitoring inputs and

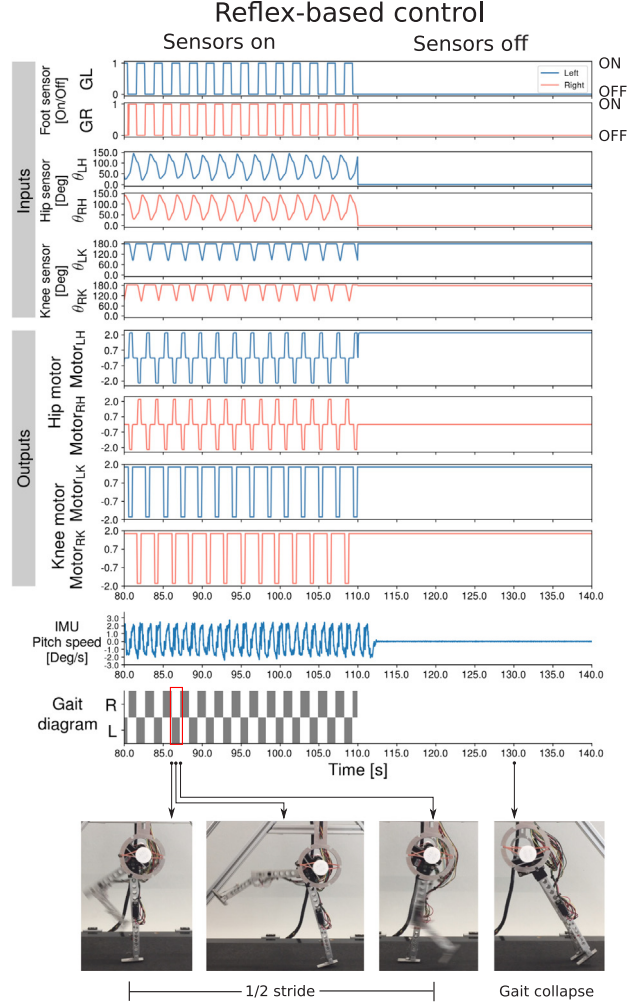


Fig. 7. The experimental results of the reflex-based control module under normal operation and in the absence of sensors. From the beginning, the robot walked with the control inputs from foot contact and joint angle feedbacks, whereas the results show only the last 30 s before sensor malfunction (i.e., with foot contact sensors off and hip and knee sensor signals set to certain values). In the absence of feedback information, the reflex-based control module could no longer generate motor driving signals (outputs). Consequently, both robot legs were paralyzed, and the robot was unable to walk as shown in the snapshot (see also Video link: www.manoonpong.com/RAS2020/SuppleVideo1.mp4). The gait diagram shows the patterns between the time periods when the robot walked steadily (left and right legs show clear swing and stance phases) and failed to walk (i.e., left and right legs could not perform clear swing and stance phases). White and gray bars show the swing and stance phases, respectively. An additional inertial measurement unit (IMU) was also attached to the body to indicate the relevant time periods. During walking, the IMU signal shows a periodic pattern due to the robot-ego motion. The IMU signal remained constant when the robot failed to walk.

generating outputs according to certain input properties. When sensory feedback is provided, the module begins its adaptation period. During this time, each feedback is transformed, becoming an input for the AFDC oscillator ($F_{CPG, L}$, $F_{CPG, R}$). In our experiment, the $H_{1, out}$ signals from the left and right CPGs were in phase from the start, then after learning, we could see that the left and right $H_{1, out}$ signals were 180° out of phase indicating a bipedal gait, and resulting in the CPG adaptation process. Accordingly, it took only around 38 s (from 55 to 93 s) for the internal CPG frequency to change, starting at an arbitrary measure of e.g., 0.77 Hz, adapted by a reduction to the external frequency of 0.45 Hz (in 5 s the robot can walk two steps/leg). When the reflexed-based control module failed and the controller switched instead to the

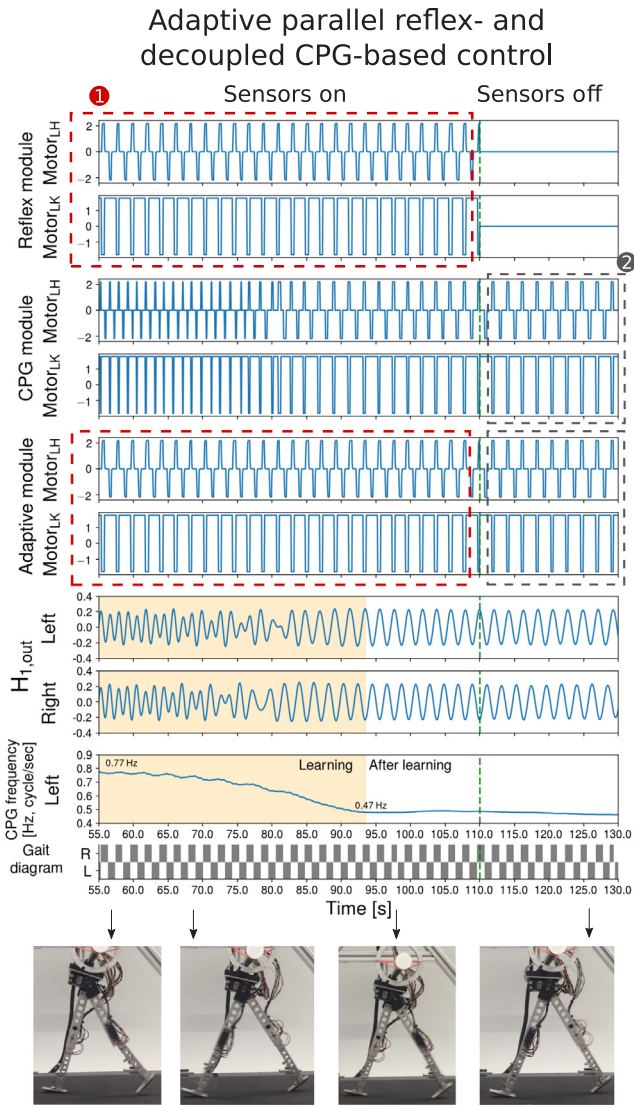


Fig. 8. The experimental results of our proposed adaptive parallel reflex- and decoupled CPG-based control module under normal operation and in the absence of sensors. The robot walked with active foot contact and joint angle feedback from the start until 55 s (when entering the yellow region) before the input was introduced into the decoupled CPG-based control module. The time lapse of 55–93 s (yellow region), represents the learning period required for the CPG signals ($H_{1, \text{out}}$) to adapt the frequency to that of the external signals ($\theta_{\text{LH}}, \theta_{\text{RH}}$). After 110 s (green line), all sensors were switched off, causing the reflex-based control module to malfunction. However, since our decoupled CPG-based control module was active, it still generated hip and knee motor signals, enabling the robot to walk uninterrupted. The final motor signals from our adaptive control consist of reflex module signals during sensor availability (number 1) and those of the CPG module during unavailability of the sensors (number 2) (Video link: www.manoonpong.com/RAS2020/SuppleVideo2.mp4). (For interpretation of the references to color in this figure legend, the reader is referred to the web version of this article.)

motor driving signals generated from the decoupled CPG-based control module, in general, the perturbation signal could still be present, such that the system continuously adapted. However, our proposed controller, demonstrated that without a perturbation signal the bipedal robot was still able to walk. This was evidenced by the driving motor signals being almost the same as the normal walking pattern. In other words, during this time, the robot could continuously and autonomously walk without any external sensory feedback and used only the internal rhythmic mechanism.

3.1.2. Speed adaptation

Our proposed control system has the ability to adapt to various walking frequencies (speeds). In other words, it can learn and generate various walking frequencies (speeds) with respect to environmental changes.

We performed the experiment under different treadmill speeds. Our reflex- and decoupled CPG-based control module operated in parallel with the reflex part to create a proper walking signal pattern for the CPG part. The results in Fig. 9 mainly show the signals from the decoupled CPG module. Each synaptic neuron H_2 (Fig. 6) sensed the hip movement and produced signals with small amplitude $H_{2, \text{out}}$ (Fig. 6), so that they transferred information to the main neurons producing $H_{0, \text{out}}$ (Fig. 6) and $H_{1, \text{out}}$ (Fig. 6). Firstly, the CPGs started with their own internal frequency of approximately 0.77 Hz in each module controlling the left leg and right leg, respectively. At this time, the treadmill operated with a constant speed 1 (0.21 m/s). When enabling the CPG inputs ($F_{\text{CPG}, L}, F_{\text{CPG}, R}$) to learn the sensory feedback from hip sensors ($\theta_{\text{LH}}, \theta_{\text{RH}}$), their frequency changed to 0.45 Hz which was the walking speed of the robot on the treadmill. We subsequently increased the speed of the treadmill to 2 (0.37 m/s), and the frequency also increased to a new value of 0.53 Hz within around 6 s. This time, our bipedal robot was in the running posture and there were small periods during which the two feet did not touch the ground.

3.2. Asymmetric conditions

In addition to normal or symmetric conditions where both legs were roughly identical, an experiment was conducted to test the robustness and performance of our proposed controller under asymmetric conditions such as the situation when the robot had unbalanced-weighted and asymmetrical elastic-resistant legs.

In all conditions, the robot had to walk in the same mode; the reflex-based mode within the first 55 s and the next 55 s during a learning period, and finally in the last 55 s our proposed decoupled CPG-based control was applied without perturbation and other sensory feedback. The hardware setup is shown in Fig. 10 with an extra weight attached to one leg and in a rubber band on the other.

3.2.1. Unbalanced-weighted leg adaptation

Several small metal blocks of 26 g each were packed to obtain 183 g, and with the addition of a nut the total weight was totally 197 g. Either the left or right leg was weighted as the robot walked on the treadmill. The results are illustrated in Fig. 11. The signals show that when either the left or right leg was equipped with the metal weight the robot could still walk with only a slight difference in its normal gait. While the foot contact and hip joint angle sensors worked properly, the reflex-based control was able to handle unbalanced conditions and the decoupled-CPG-based control could uninterruptedly take over when all sensors were not working.

3.2.2. Asymmetrical elastic resistance adaptation

We tested the situation where the elasticity at each leg was not equal. One leg was exerted by a rubber band with a spring constant of K 39.4 N/m (or Young's modulus 0.0005 GPa) at a time. The results are shown in Fig. 12. The rubber band resisted one of the robot's upper legs during the swing phase and accelerated backward during the stance phase of the same leg, causing a slight slip. However, the hip and foot sensory signals show no significant difference from the normal gait. Regarding the walking frequency, we did the test where the rubber band was fastened onto either one of the legs, then the frequencies of both legs were measured. It turned out that both legs still swung with

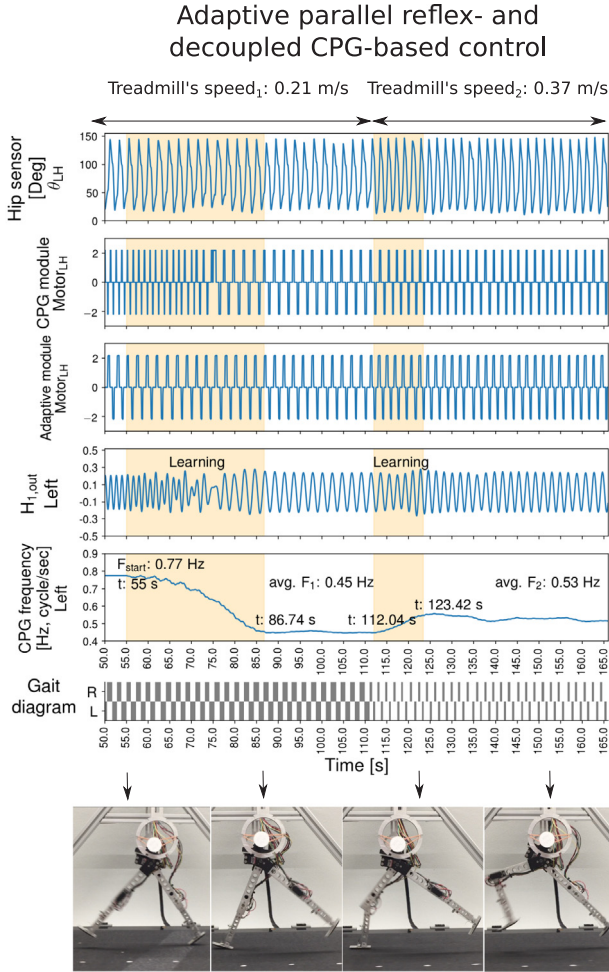


Fig. 9. Experimental results of our proposed adaptive parallel reflex- and decoupled CPG-based control module under different treadmill speeds when the robot is operated using the adaptive module. The reflex-based module was active and tracked the treadmill speed. In parallel, the decoupled CPG-based control module could adapt to different external speeds by learning the hip sensor signal (e.g., θ_{LH}) as feedback. The CPG frequency graph of the $H_{1,out}$ signal shows its ability to adapt to different speeds, generating the proper motor signals for driving the hips (e.g., $Motor_{LH}$) and knees (Video link: www.manoonpong.com/RAS2020/SuppleVideo3.mp4).

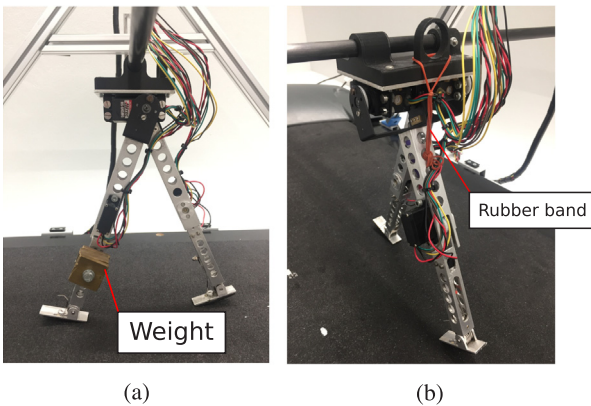


Fig. 10. The two different hardware conditions in the robustness and performance assessment: (a) DACBOT with extra weight in one leg; (b) DACBOT with a rubber band representing elastic resistance in one leg.

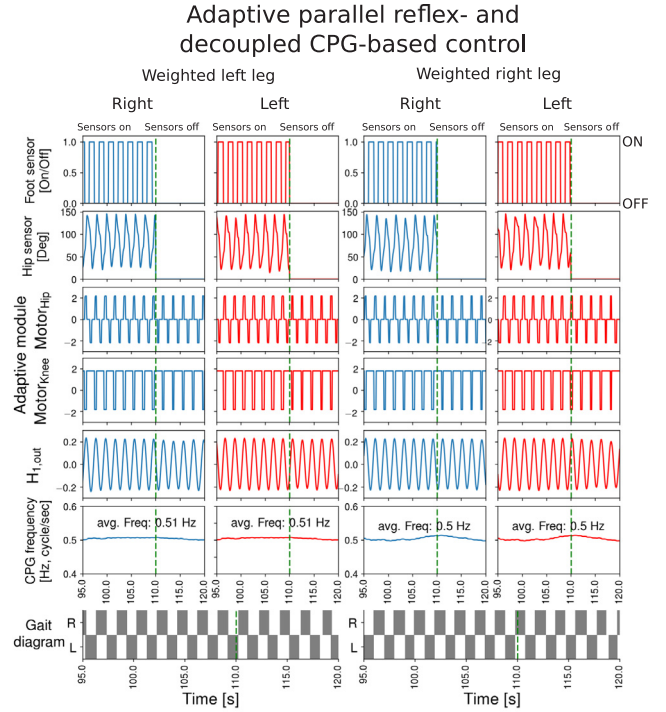


Fig. 11. The experimental results of our proposed adaptive parallel reflex- and decoupled CPG-based control module with an unbalanced leg under normal conditions and in the absence of sensors. Our controller could handle both situations whereby the weight was attached on either the left or right leg. It is interesting to note that even though one leg has more weight than the other, the frequencies of both legs are almost the same. This is due to the intrinsic coupling of the mechanical structure between the legs resulting in global walking dynamics (i.e., both legs move within the same frequency range); thereby enabling the robot to walk (Video link: www.manoonpong.com/RAS2020/SuppleVideo4.mp4).

nearly the same frequency on the average. However, there might be slight differences between the tightened-left and-right leg situations. Since we did not fasten the rubber band at the exact same location between these two situations, this may cause the band length to differ, resulting in differences in the force of the spring. This accords with $F = kx$ whereby the spring constant k is the same, but length x is slightly different. Therefore, this slight difference in force may lead to a slightly different response of the walking frequency (Fig. 12 from 0.55 to 0.49 Hz).

4. Discussion and conclusions

Based on the experiments, our proposed control framework for complex bipedal locomotion with the utilization of an adaptive parallel reflex- and decoupled CPG-based control module shows that the robot could perform stable gait generation in the sagittal plane. The hip motor signal generated from our control module indicates certain periods when the driving voltage is zero (hip motor in Fig. 5), enabling the robot to move with minimal energy consumption. Our neural based approach can handle bipedal locomotion efficiently.

This reflex-based control module composed of flexion, extension, and sensory neurons can successfully integrate all constituents of the robot's entity to interact with its environment in a specific way; in our case, to generate a certain gait. However, only the reflex-based module has limitations when some sensory feedback are absent, causing unstable movement.

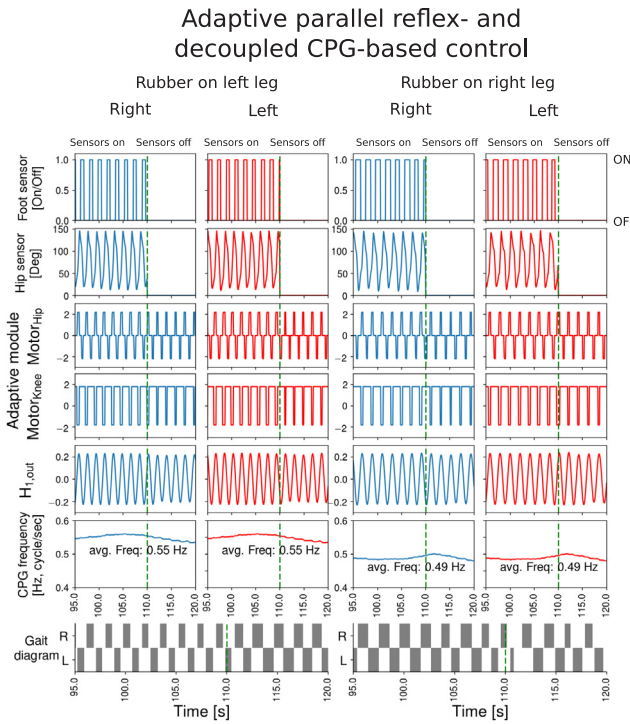


Fig. 12. The experimental results of our proposed adaptive parallel reflex- and decoupled CPG-based control module with asymmetrical elastic resistance under normal conditions, in the absence of sensors. Our controller could handle situations in which the elasticity on each leg was not equal by resisting either the left or right leg with a rubber band fastened to the upper leg. We also show here the slightly different responses of the walking frequency due to varying elastic values when fastening the rubber band. The different elastic value in one leg causes a change in the swing period of that leg which in turn also affects the walking dynamics of the other leg through the intrinsic coupling of the mechanical structure between the legs. This results in global walking dynamics (i.e., both legs move within the same frequency range); thereby enabling the robot to walk (Video link: www.manoonpong.com/RAS2020/SuppleVideo5.mp4).

A previous study on the use of one CPG-based control module mitigated this issue by acting as the auxiliary controller whereby the online learning property acquires sensory feedback from a joint angle, generating a rhythmic signal when the main reflex-based control fails. Nevertheless, although the design relies on information from one leg [15], it uses this to control both legs, and does not reflect the practical situation where each leg can experience different asymmetric conditions (such as unbalanced weight and asymmetric elastic resistance in the legs). Our new control approach with the decoupled CPG-based controller, where each CPG controls each leg individually, is flexible and efficient for bipedal locomotion generation with the side supports (i.e., locomotion in the sagittal plane). Thus, it can be later applied to lower-limb exoskeletons for rehabilitation with support (e.g., parallel bars or crutches). The benefit of this approach is that it expresses robustness during sensory feedback malfunction. The main control (reflex-based module) is employed for gait generation with the auxiliary control (decoupled CPG-based module) for memorizing and maintaining the gait during a sensory malfunction situation or to reproduce the original gait as desired. This allows the robot to continuously walk. Practically, the ability of the control to handle the sensory malfunction is crucial for safety purposes in subsequent application to an exoskeleton when the reflex-based module can be replaced by a human or redesigned to cooperate with a human. From the CPG perspectives, these AFDCs obviously express adaptive online learning properties, as

demonstrated in the speed adaptation experiment in which the controller could acknowledge the various abrupt speed changes in a few seconds. Furthermore, it can handle situations in which both legs are asymmetric, such as weight imbalance or asymmetric elastic resistance. Even though the reflex-based module can handle asymmetric conditions, in the absence of the decoupled CPG-based module we cannot gain insight into the walking frequency of each leg in an online manner which will be useful for further work involving human walking. The adaptation and asymmetry compensation of the control will be useful for applying to the exoskeleton for rehabilitation in stroke patients who walk with a limp.

However, there are limitations to this study and further aspects need to be explored. Sensory feedbacks in this case consist of foot contact and joint angle sensor signals. The reflex-based module will not work if either sensor fails. The decoupled CPG-based module then takes over to maintain robot locomotion. If the hip sensors fail, the CPGs will receive no input. Consequently, the decoupled CPG-based module becomes open-loop following deployment. This means that the significant changes in speed, mass, or elasticity will cause the gait to collapse. Nevertheless, since the CPG has a limit cycle, it can tolerate a certain amount of disturbance or minor changes. On the contrary, if the reflex-based module fails in such a way that the hip sensors remain working, the CPG module can still work in a closed-loop manner for further gait adaptation. This issue will be investigated in future study. Furthermore, we will apply the control approach to a lower-limb exoskeleton system for assistance and rehabilitation. Within this assistive walking application, a trajectory shaping method [33] and compliant motor control [34] will also be investigated and integrated into the proposed adaptive control framework for natural locomotion and smooth gait transition.

Declaration of competing interest

The authors declare that they have no known competing financial interests or personal relationships that could have appeared to influence the work reported in this paper.

Acknowledgments

We would like to thank the University of Southern Denmark for its kind cooperation. This work has also been supported by the startup IST flagship research grant from Vidyasirimedhi Institute of Science & Technology (VISTEC), Thailand and PTT-RAII, Thailand under the adVanced human-machIne interactionS technology for impRoving quAlity of life and health (VIS-RA) project.

References

- [1] N. Kashiri, A. Abate, S.J. Abram, A. Albu-Schaffer, P.J. Clary, M. Dally, S. Faraji, R. Furnemont, M. Garabini, H. Geyer, A.M. Grabowski, J. Hurst, J. Malzahn, G. Mathijssen, D. Remy, W. Roozing, M. Shahbazi, S.N. Simha, J.-B. Song, N. Smit-Anseeuw, S. Stramigioli, B. Vanderborght, Y. Yesilevskiy, N. Tsagarakis, An overview on principles for energy efficient robot locomotion, *Front. Robot. AI* 5 (2018) 129.
- [2] L. Meng, C.A. Macleod, B. Porr, H. Golle, Bipedal robotic walking control derived from analysis of human locomotion, *Biol. Cybernet.* 112 (3) (2018) 277–290.
- [3] P. Arena, L. Patané, D. Sanalitro, A. Vitanza, Insect-Inspired Body Size Learning Model on a Humanoid Robot, in: 2018 7th IEEE International Conference on Biomedical Robotics and Biomechatronics, Biorob, 2018, pp. 1127–1132.
- [4] N. Van der Noot, A.J. Ijspeert, R. Ronsse, Neuromuscular model achieving speed control and steering with a 3D bipedal walker, *Auton. Robots* 43 (6) (2019) 1537–1554.

- [5] S. Kajita, F. Kanehiro, K. Kaneko, K. Fujiwara, K. Harada, K. Yokoi, H. Hirukawa, Biped walking pattern generation by using preview control of zero-moment point, in: 2003 IEEE International Conference on Robotics and Automation (Cat. No.03CH37422), Vol. 2, 2003, pp. 1620–1626.
- [6] Y. Hong, J. Kim, 3-D command state-based modifiable bipedal walking on uneven terrain, *IEEE/ASME Trans. Mechatronics* 18 (2) (2013) 657–663.
- [7] S. Kuindersma, F. Permenter, R. Tedrake, An efficiently solvable quadratic program for stabilizing dynamic locomotion, in: 2014 IEEE International Conference on Robotics and Automation, ICRA, 2014, pp. 2589–2594.
- [8] D.J. Braun, J.E. Mitchell, M. Goldfarb, Actuated dynamic walking in a seven-link biped robot, *IEEE/ASME Trans. Mechatronics* 17 (1) (2012) 147–156.
- [9] O. Tutsoy, CPG based RL algorithm learns to control of a humanoid robot leg, *Int. J. Robot. Autom.* 30 (2) (2015) 178–183, Publisher: IASTED.
- [10] T. Geng, B. Porr, B. Florentinwörgötter, A reflexive neural network for dynamic biped walking control, *Neural Comput.* 18 (5) (2006) 1156–1196.
- [11] H. Geyer, H. Herr, A muscle-reflex model that encodes principles of legged mechanics produces human walking dynamics and muscle activities, *IEEE Trans. Neural Syst. Rehabil. Eng.* 18 (3) (2010) 263–273, Conference Name: IEEE Transactions on Neural Systems and Rehabilitation Engineering.
- [12] A.J. Ijspeert, Central pattern generators for locomotion control in animals and robots: A review, *Neural Netw.* 21 (4) (2008) 642–653.
- [13] G. Taga, Y. Yamaguchi, H. Shimizu, Self-organized control of bipedal locomotion by neural oscillators in unpredictable environment, *Biol. Cybernet.* 65 (3) (1991) 147–159.
- [14] F. Dzeladini, J. van den Kieboom, A. Ijspeert, The contribution of a central pattern generator in a reflex-based neuromuscular model, *Front. Hum. Neurosci.* 8 (2014).
- [15] G.D. Canio, S. Stoyanov, I.T. Balmori, J.C. Larsen, P. Manoonpong, Adaptive combinatorial neural control for robust locomotion of a biped robot, in: From Animals to Animats 14, in: Lecture Notes in Computer Science, Springer, Cham, 2016, pp. 317–328.
- [16] Y. Huang, Q. Wang, Disturbance rejection of central pattern generator based torque-stiffness-controlled dynamic walking, *Neurocomputing* 170 (2015) 141–151.
- [17] P. Manoonpong, T. Geng, T. Kulvicius, B. Porr, F. Wörgötter, Adaptive, fast walking in a biped robot under neuronal control and learning, *PLoS Comput. Biol.* 3 (7) (2007) 1–16.
- [18] K. Matsuoka, Sustained oscillations generated by mutually inhibiting neurons with adaptation, *Biol. Cybernet.* 52 (6) (1985) 367–376.
- [19] G.L. Liu, M.K. Habib, K. Watanabe, K. Izumi, Central pattern generators based on Matsuoka oscillators for the locomotion of biped robots, *Artif. Life Robot.* 12 (1) (2008) 264–269.
- [20] G. Endo, J. Morimoto, J. Nakanishi, G. Cheng, An empirical exploration of a neural oscillator for biped locomotion control, in: IEEE International Conference on Robotics and Automation, 2004. Proceedings. ICRA '04. 2004, Vol. 3, 2004, pp. 3036–3042.
- [21] G. Endo, J. Nakanishi, J. Morimoto, G. Cheng, Experimental Studies of a Neural Oscillator for Biped Locomotion with QRIO, in: Proceedings of the 2005 IEEE International Conference on Robotics and Automation, 2005, pp. 596–602.
- [22] T. Matsubara, J. Morimoto, J. Nakanishi, M. Sato, K. Doya, Learning CPG-based biped locomotion with a policy gradient method, in: 5th IEEE-RAS International Conference on Humanoid Robots, 2005., 2005, pp. 208–213.
- [23] O. Tutsoy, D. Erol Barkana, S. Colak, Learning to balance an NAO robot using reinforcement learning with symbolic inverse kinematic, *Trans. Inst. Meas. Control* 39 (11) (2017) 1735–1748, Publisher: SAGE Publications Ltd STM.
- [24] Y. Nakamura, T. Mori, M.-a. Sato, S. Ishii, Reinforcement learning for a biped robot based on a CPG-actor-critic method, *Neural Netw.* 20 (6) (2007) 723–735.
- [25] E. Yazdi, A.T. Haghhighat, Evolution of biped walking using neural oscillators controller and harmony search algorithm optimizer, 2010, [arXiv:1006.4553](https://arxiv.org/abs/1006.4553) [cs].
- [26] A.A. Saputra, J. Botzheim, I.A. Sulistijono, N. Kubota, Biologically inspired control system for 3-D locomotion of a humanoid biped robot, *IEEE Trans. Syst. Man Cybern: Syst.* 46 (7) (2016) 898–911.
- [27] L. Righetti, J. Buchli, A.J. Ijspeert, Dynamic Hebbian learning in adaptive frequency oscillators, *Physica D* 216 (2) (2006) 269–281.
- [28] C.P. Santos, N. Alves, J.C. Moreno, Biped locomotion control through a biomimetic CPG-based controller, *J. Intell. Robot. Syst.* 85 (1) (2017) 47–70.
- [29] T. Nachstedt, C. Tetzlaff, P. Manoonpong, Fast dynamical coupling enhances frequency adaptation of oscillators for robotic locomotion control, *Front. Neurorobot.* 11 (2017) 14.
- [30] A.D. Kuo, The relative roles of feedforward and feedback in the control of rhythmic movements, *Motor Control* 6 (2) (2002).
- [31] P. Manoonpong, T. Kulvicius, F. Wörgötter, L. Kunze, D. Renjewski, A. Seyfarth, Compliant ankles and flat feet for improved self-stabilization and passive dynamics of the biped robot "RunBot", in: 2011 11th IEEE-RAS International Conference on Humanoid Robots, 2011, pp. 276–281.
- [32] F. Pasemann, M. Hild, K. Zahedi, SO(2)-networks as neural oscillators, in: J. Mira, J.R. Álvarez (Eds.), *Computational Methods in Neural Modeling*, Springer Berlin Heidelberg, Berlin, Heidelberg, 2003, pp. 144–151.
- [33] M. Pitchai, X. Xiong, M. Thor, P. Billeschou, P.L. Mailänder, B. Leung, T. Kulvicius, P. Manoonpong, CPG driven RBF network control with reinforcement learning for gait optimization of a dung beetle-like robot, in: I.V. Tettko, V. Kurková, P. Karpov, F. Theis (Eds.), *Artificial Neural Networks and Machine Learning - ICANN 2019: Theoretical Neural Computation*, Springer International Publishing, Cham, 2019, pp. 698–710.
- [34] X. Xiong, F. Wörgötter, P. Manoonpong, Virtual agonist-antagonist mechanisms produce biological muscle-like functions: An application for robot joint control, *Ind. Robot: Int. J. Robot. Res. Appl.* 41 (4) (2014) 340–346.



Chaicharn Akkawutvanich received a M.Sc. degree in Biomedical Engineering from the RWTH Aachen University, Aachen, Germany, in 2012. He is currently pursuing a Ph.D. degree with School of Information Science & Technology at Vidyasirimedhi Institute of Science & Technology (VISTEC), Thailand. His current research interests include exoskeletons, prosthetic and orthopedic, machine learning, and human-machine interaction.



Frederik Ibsgaard Knudsen received a B.Sc. in Robot Systems from the University of Southern Denmark, Odense, Denmark in 2019. He is currently pursuing a M.Sc. degree in Robot System at the University of Southern Denmark and is employed as a student assistant with SDU Embodied Systems for Robotics and Learning. His current research interests include embodied AI, beneficial AI, machine learning, learning/plasticity, collaborative robotics, and design of bipedal robotic systems.



Anders Falk Riis received a B.Sc. in Robot Systems from the University of Southern Denmark, Odense, Denmark in 2019. He currently works for an international engineering corporation focusing on artificial intelligence, computer vision, robotics and electronics. He is employed to develop on their software and computer vision. Further interests are AI, machine learning and neural network.



Jørgen Christian Larsen received his B.Eng degree in Science in Computer Systems Engineering in 2008 from the Mærsk Mc-Kinney Møller Institute, University of Southern Denmark, and a M.Sc. degree in Robot Systems Engineering 2011, from the Mærsk Mc-Kinney Møller Institute, University of Southern Denmark. Simultaneously with studying for the master degree, he also started working as a Ph.D. student on the EU Project Locomorph, which resulted in a Ph.D. degree in Robotic Systems in 2013 also from the Mærsk Mc-Kinney Møller Institute, University of Southern Denmark. Currently, he is an Associate Professor in Embedded electronics and Artificial Intelligence at the University of Southern Denmark. He is also an Adjunct Professor at the School of Information Science & Technology at Vidyasirimedhi Institute of Science & Technology (VISTEC), Thailand. His research interests cover areas from embodied artificial intelligence, embedded electronics, FPGA control and design, and cyber-physical systems, mechanical design of walking machines, soft robotics, and educational research.



Poramate Manoonpong received a Ph.D. degree in Electrical Engineering and Computer Science from the University of Siegen, Siegen, Germany, in 2006. He was the Emmy Noether Research Group Leader for Neural Control, Memory, and Learning for Complex Behaviors in Multisensory-Motor Robotic Systems with the Bernstein Center for Computational Neuroscience, Georg-August Universität Göttingen, Göttingen, Germany, from 2011 to 2014. Currently, he is a Professor of School of Information Science & Technology at Vidyasirimedhi Institute of Science & Technology (VIS-

TEC), Thailand. He has also served as an Associate Professor of Embodied AI & Robotics at the University of Southern Denmark (SDU), Denmark and a Professor at the College of Mechanical and Electrical Engineering at Nanjing University of Aeronautics and Astronautics (NUAA), China. His current research interests include embodied AI, machine learning for robotics, neural locomotion control of walking machines, biomechanics, dynamics of recurrent neural networks, learning/plasticity, embodied cognitive systems, prosthetic and orthopedic devices, exoskeletons, brain-machine interface, human-machine interaction, and service/inspection robots.